The impact of lipid polyunsaturation on the physical and mechanical properties of lipid membranes

Rim Baccouch, Yarong Shi, Emilie Vernay, Marion Mathelié-Guinlet, Nada Taib-Maamar, Sandrine Villette, Cecile Feuillie, Estelle Rascol, Philippe Nuss, Sophie Lecomte, et al.

The impact of lipid polyunsaturation on the physical and mechanical properties of lipid membranes

Rim Baccouch[1a], Yarong Shi[2a], Emilie Vernay[1], Marion Mathelié-Guinlet[1], Nada Taib-Maamar[1], Sandrine Villette[1], Cécile Feuillie[1], Estelle Rascol[1], Philippe Nuss[3, 4], Sophie Lecomte[1], Michael Molinari[1], Galya Staneva[5], Isabel D. Alves[1*]

[1] Univ. Bordeaux, CNRS, Bordeaux INP, CBMN, UMR 5248, Bat B14, allée Geoffroy St. Hilaire F-33600 Pessac, France; [2] Laboratoire de Recherche en Nanosciences, LRN EA4682, University of Reims Champagne Ardenne, France; [3]Centre de Recherche Saint-Antoine, INSERM UMRS 938, Sorbonne Université, Paris, France; [4]Service de psychiatrie et de psychologie médicale, Sorbonne Université, Hôpital Saint-Antoine, AP-HP, Paris, France; [5]Institute of Biophysics and Biomedical Engineering, Bulgarian Academy of Sciences, Acad. G. Bonchev Str., Bl.21, 1113 Sofia, Bulgaria; [a]authors have equally contributed to this work; *corresponding author: i.alves@cbmn.u-bordeaux.fr

The lipid composition of cellular membranes and the balance between the different lipid components can be impacted by aging, certain pathologies, specific diets and other factors. This is the case in a subgroup of individuals with psychiatric disorders, such as schizophrenia, where cell membranes of patients have been shown to be deprived in polyunsaturated fatty acids (PUFAs), not only in brain areas where the target receptors are expressed but also in peripheral tissues. This PUFA deprivation thus represents a biomarker of such disorders that might impact not only the interaction of antipsychotic medications with these membranes but also the activation and signaling of the targeted receptors embedded in the lipid membrane. Therefore, it is crucial to understand how PUFAs levels alterations modulate the different physical properties of membranes.

In this paper, several biophysical approaches were combined (Laurdan Fluorescence Spectroscopy, Atomic Force Microscopy, Differential Scanning Calorimetry, Molecular Modeling) to characterize membrane properties such as fluidity, elasticity and thickness in PUFA-enriched cell membranes and lipid model systems reflecting the PUFA imbalance observed in some diseases. The impact of both the number of unsaturations and their position along the chain on the above properties was investigated. Briefly, data revealed that PUFA presence in membranes increases membrane fluidity, elasticity and flexibility and decreases its thickness and order parameter. Both the level of unsaturation and their position affect these membrane properties.

Keywords: polyunsaturated fatty acids; lipid membrane physico-chemical properties; fluidity; lipid phase transition temperature; thickness.

1. Introduction

Membranes contain over one thousand different lipid species, yet, besides few exceptions, the clear function of each species remains greatly unknown. Among those, phospholipids constitute the major family and while most cellular membranes contain saturated and monounsaturated acyl chains, certain organs like the brain possess about 30% of polyunsaturated fatty acid phospholipids (PUFA-PLs) with synaptic vesicles containing up to 80% of phospholipids with at least one polyunsaturated acyl chain [1], [2].

PUFAs are fatty acid chains with 20-22 carbons in length that contain 2-6 *cis* double bonds and are divided into two subclasses, ω3 and ω6, depending on the position of the first double bond (when going from the carbon atom that is more distant from the phospholipid headgroup). The most common PUFAs are arachidonic acid (AA) and docosahexaenoic acid (DHA), AA being ω6 with 4 unsaturations (C22:4 n-6) and DHA being ω3 with 6 unsaturations (C22:6 n-3) (the abbreviation indicates the number of carbons, the number of double bonds and the position of the first double bond relative to the terminal methyl).

Except for mead acid, which is an ω9 PUFA (C20:3 n-9), PUFAs cannot be synthesized endogenously in mammals. The α-linolenic acid (ALA, C18:3 n-3) or linoleic acid (LA, C18:2 n-6) are essentials fatty acids because they cannot be synthesized *de novo* and can only be obtained from diet. The other PUFAs can theoretically be converted from these two precursors, EPA from ALA and AA from LA, but the conversion rate is very low for DHA which is also considered as essential. The metabolic pathways implicated in the biosynthesis of the different PUFAs can be found elsewhere [3]. Once synthesized they are incorporated in different phospholipids, but preferentially in phosphatidylcholine (PC), phosphatidylethanolamine (PE) and phosphatidylserine (PS) [4]–[6], via acyltransferases. The dietary intake of ω3 like DHA or eicosapentaenoic acid (EPA; C20:5 n-3) have been associated with beneficial effects on cardiovascular and neurological systems [7]–[10] and with an anti-inflammatory action [11].

The importance of PUFAs in the structural and functional maintenance of the central nervous system is further evidenced by the correlation between a deficiency in brain PUFA levels (like DHA and EPA) and numerous psychiatric disorders as observed in clinical pilot programs [12]–[14] and *post-mortem* analysis in psychiatric patients [15]–[17]. Remarkably, Ducrocq et al established a causal link not only between nutritional deficiency in PUFA-ω3 and the appearance of motivational disorders associated with several psychiatric disorders but also with the alteration of dopaminergic transmission [18].

This work has shown, for the first time, that the restoration of PUFA-ω3 content in neurons expressing dopamine D2 receptor (D2R) prevented the onset of motivational disorders caused by PUFA deficiency.

The positive correlation between psychiatric disorders and a deficiency in PUFA-ω3 levels raises an important question: how do variations in PUFA levels modulate the physical and mechanical properties of lipid membranes and subsequently impact the activity of embedded proteins?

The work presented herein aims at shedding light into this question, by employing both: 1) cellular systems enriched with different fatty acids in order to mimic physio-pathological conditions; 2) lipid model membranes containing or not PUFA-PLs. In both approaches, ω3 and ω6 type PUFA in their free form and PUFA-PLs containing a varying number of unsaturation will be used. This strategy aims at disentangling the role of both the number and the position of the unsaturation in the membrane physico-chemical properties, such as thickness, elasticity, fluidity, phase transition temperature, order and curvature.

While several research teams have reported on the impact of membrane PUFA levels in certain membrane properties like: elasticity, bending rigidity, fluidity, membrane domain stability, thickness, phase transition temperature (to cite a few references [6], [19]–[25]), a systematic study and parallel comparison of different PUFAs at levels that reflect those occurring in pathophysiological conditions is still missing.

Using both experimental (AFM, Calorimetry, Laurdan fluorescence, Raman) and theoretical approaches (Molecular Modeling) in cellular and model membranes we have investigated the impact of the number and the position of the double bonds membrane behavior.

2. Materials and Methods

2.1. Materials

Docosahexaenoic Acid (DHA, Sigma-Aldrich), Arachidonic acid (AA, Sigma-Aldrich), Docosapentaenoic acid (ω3 and ω6 DPA, Sigma-Aldrich), Docosahexaenoic Acid Alkyne (DHA-Alkyne, Cayman Chemical), were prepared in ethanol under nitrogen flux at 30mM concentration and stored as aliquots at -80°C. Cholesterol, POPC, SAPC, SDhaPC, DPPC and DSPC, all from Avanti Lipids, were obtained either in powder or in chloroform. The membrane fluorescent probe Laurdan (6-dodecanoyl-2-dimethylaminonaphthalene) was obtained from ThermoFisher, dissolved in 100% dimethylsulfoxide (DMSO) at 5 mM concentration and kept

in long-term storage at -20°C; when needed for experiments, aliquots were kept at 4°C for at most 4 weeks.

2.2. Cell culture and PUFA cell enrichment

HEK-293 human embryonic kidney cells were cultivated with Dulbecco's modified Eagle's medium (DMEM), high glucose, supplemented with glutamax and pyruvate (Gibco, 31966-021), 10% of fetal bovine serum (Sigma-Aldrich, F9665), 1% antibiotics (penicillin/streptomycin, Sigma-Aldrich, P433) at 37°C in a 5% CO_2 incubator.

For Raman experiments, before measurement, cells were seeded at 5×10^4 cells/well on poly-L-lysine (Sigma-Aldrich, P4707) coated glass cover slides deposited in 4-wells plates (1.9 cm^2 well area). The next day, the medium was replaced with fresh DMEM supplemented with 30 µM of PUFA (0.1% ethanol for control cells). After 24h of incubation, cells were rinsed three times with DMEM, then washed with phosphate buffer saline (PBS) and fixed with 4% formaldehyde (Thermo Scientific) for 20 minutes at room temperature. Fixed cells were rinsed successively with increasingly diluted PBS solution (100% PBS, 75%-25% PBS/water, 50%-50% PBS/water, 25%-75% PBS/water, 10%-90% PBS/water) to remove most of the salts without inducing osmotic cell damage before drying the cells under a soft nitrogen flux. Cells were observed within 5 days of fixation and drying.

For Laurdan experiments, freshly splitted HEK-293 cells were plated into 6-well plates at a density of 3×10^5 cells per well and cultured for 24 hours in complete DMEM. The next day, HEK cells were enriched with the PUFA of interest (DHA, DPA-ω3, DPA-ω6, AA) as described above (section 2.2). 24 h after PUFA treatment, both control and enriched cells were rinsed with preheated PBS buffer (37°C), collected and centrifuged at 1500 rpm for 5 min. After two centrifugal washing steps with PBS, cells were resuspended to a final concentration of 1.2×10^6 cells per mL and incubated for 60 min with Laurdan which was added to the cell suspension at final concentration of 10 µM. During the staining step, control and PUFA-enriched cells were kept in a temperature and CO_2 controlled chamber to maintain optimum physiological conditions and to avoid any biased changes in membrane fluidity. Suspensions of labeled cells were washed twice by centrifugation at 1500 rpm for 5 min and resuspended in prewarmed PBS. Finally, cells suspensions (100µL) were aliquoted in triplicate into flat bottom black 96-well plate and the Generalized Polarization (GP) values of cells suspensions were calculated to determine cell membrane order as described in section 2.6.

2.3. Preparation of model lipid membranes

For DSC experiments, DPPC-containing liposomes were prepared as followed. DPPC dissolved in chloroform and PUFAs dissolved in ethanol, either as free form (AA, DHA, DPA-ω3 and DPA-ω6) or embedded within a phospholipid (SAPC, SDhaPC)), were pipetted into an Eppendorf in appropriate volumes to reach a molar ratio of 9:1 and stirred to get homogeneous solutions. The solvents were first removed by evaporation at room temperature under a nitrogen stream.

The samples were then placed under vacuum in a desiccator for 2h to ensure complete evaporation of organic solvent. The thin lipid film obtained on the inside wall of the Eppendorf was rehydrated with a Tris buffer solution (50 mM TrisHCl, NaCl 500 Mm, pH 8) to reach a final concentration of 1 mg/mL of lipids. Finally, the lipid suspensions were highly vortexed until total dissolution for complete homogenization and stored at 4°C until further use, for 2-weeks maximum.

For Laurdan experiments, liposomes were prepared by mixing lipids at the appropriate ratios with chloroform/methanol (2:1 v/v). The Laurdan labelling procedure was done by premixing the fluorescent probe with the lipid fraction to obtain a probe to lipid ratio of 1:200 (mol/mol). A lipid film was obtained after solvent evaporation under nitrogen stream. The dried lipid/dye mixture was then hydrated with 50 mM Tris/150 mM NaCl buffer at pH 7.4 to yield a lipid concentration of 1 mM. The lipid suspension was then incubated for 10 min at 60 °C, gently vortexed and sonicated for 2 min. To create Multi Lamellar Vesicles (MLVs), the lipid suspension was subjected to three freeze –thaw cycles (liquid nitrogen–water 60 °C) followed by vortexing and sonication. Labelled MLVs were kept for up to 6 days at -4°C and protected from light until use.

2.4. Raman measurements

Raman spectra were collected with an Alpha 300RS (WITec GmbH, Ulm, Germany) instrument equipped with an EMCCD high intensity low noise camera and a high precision piezoelectric scanning stage. Raman spectra were recorded using a 532 nm excitation green laser and a 600 g per mm grating. The spectral resolution was around 8 cm^{-1}. The beam was focused on the sample using an Olympus objective (100×/0.95 NA). Raman cellular mapping was performed with a step size of 1 μm and 2 s acquisition time per spectrum, with a laser power at the sample of 22 mW. Data acquisition was controlled by the WITec alpha 300

software Control FIVE. All data were processed using Projet FIVE Plus software (WITec GmbH, Ulm, Germany).

Pre-processing included cosmic ray removal (CRR) and background subtraction using a shape function (at a shape size of 250 and a noise factor of 4). Data were reduced to 400-3600 cm^{-1} range before analysis. Principal component analysis was performed on the spectral image matrix. The first 11 principal components were found significant and used to reconstruct spectra with a reduced noise.

For the analysis of the Raman spectra of dried DHA-Alkyne, one μL droplet of 30 mM fatty acid (in ethanol) was deposited on a SpectRIM slide (highly polished stainless-steel substrate with an ultra-thin hydrophobic coating that displays no appreciable Raman spectrum, Tienta Sciences) and allowed to dry for a few minutes at room temperature. Very low laser intensity (λ=532 nm) was used and at least 3 spectra at different locations were averaged using 10s acquisition time per spectrum.

2.5. Atomic force microscopy (AFM) :

AFM is a powerful high-resolution imaging tool to simultaneously observe the morphology of a sample and quantitatively measure its mechanical properties with nanoscale resolution in physiologically relevant conditions [26], [27].

Multiparametric imaging of live cells in liquid media allows obtaining correlative height images and nanomechanical properties maps, and it has notably allowed evidencing specific phenotypes in the apparent Young's modulus of cancerous cells compared to healthy ones [28].

Nanomechanical mapping on living cells was performed with a Bioscope Resolve AFM (CA Bruker) coupled to an optical inverted microscope (Axioscope, Zeiss) and a confocal microscope (Zeiss LSM-800) with a 63×/1.4 oil objective. To acquire correlative AFM images, PFQNM-LC-CAL (pre-calibrated, Bruker) tips were used in PeakForceTapping mode with Quantitative Nanomechanical analysis (QNM) at imaging forces of ~400 pN with a peak force frequency of 0.25 kHz, a 1000-nm amplitude, a 128x128 resolution and a scan rate of 0.1 Hz. Before each experiment, cantilevers were calibrated with the thermal tune method [29]. The AFM and confocal microscope were equipped with a cell-culture chamber to maintain the temperature at 37 ± 1 °C. Force-distance curves (as shown in Fig. S1A, Supplementary Information) were recorded at the perinuclear part, thick enough to avoid any effect of the substrate or the nucleus, which may influence the measurements [30]. The heterogeneity of a cell structure can lead to a broad distribution of the Young's modulus (as shown in Fig. S1B,

Supplementary Information). Therefore, a large number of measurements was considered, performed at different locations over a single cell (> 3 areas). For each condition, more than 24 cells from 3 to 6 independent samples were studied, with over 1000 force-distance curves per cell. AFM images and force curves were analyzed using Nanoscope analysis, Origin, and ImageJ.

Optical images (as shown in Fig. S1C, Supplementary Information) were acquired before and after AFM imaging to ensure the cells are still alive with no tip-induced morphological changes. If the shape of a cell has significantly changed after the AFM measurements, it is discarded from analysis.

The elastic properties of the cells were quantified based on AFM acquired force-distance curves, through calculation of their Young's modulus following the widely accepted formula [31], [32] of Sneddon's contact model [33]:

$$F = \frac{2}{\pi}\frac{E}{(1-\upsilon^2)}\tan(\alpha)\delta^2$$

where F is the indentation force, E is the Young's modulus to be determined, ν is the Poisson's ratio (related to the compressibility of the sample material), α is the half-angle of the indenter (18° in this case), and δ is indentation depth.

As reported elsewhere [33], we assumed cells to be incompressible material and used a Poisson's ratio of 0.5. Outliers above Q3 +1.5 IQ and under Q1 - 1.5 IQ (Q = quartile, IQ = Interquartile range) were discarded. Given the lognormal distributions observed, statistical significance was assessed using a non-parametric Kruskal-Wallis test with Dunn's multiple comparison test. To properly reflect the asymmetry of the data, the confidence interval at 95% have been calculated in accordance with previous literature[34] and are displayed in Table II.

2.6. Laurdan fluorescence measurements

Changes in membrane's fluidity were determined using generalized polarization (GP), a spectroscopic property of Laurdan which reflects the intensity ratio of the probe emitting at shorter (more ordered) and longer (less ordered) wavelengths. GP values were calculated according to Parasassi *et al* [35]:

$$GP = \frac{I_{440}-I_{490}}{I_{440}+I_{490}}$$

where I_{440} and I_{490} represent the fluorescence intensity emitted at 440 nm and 490 nm, respectively. Fluorescence emission spectra of Laurdan labeled membranes were measured following excitation at 360 nm using a spectrofluorometer (Tecan infinite M1000 Pro).

For each condition, Laurdan GP measurements (at least 23) were carried out from 3 independent samples.

2.7. Differential scanning calorimetry (DSC):

DSC measurements were performed with a MicroCal PEAQ-DSC (Malvern Panalytical). 250 µL of lipid suspensions at 1mg/mL were loaded into the calorimeter in the form of multilamellar vesicles prepared as described above. Four heating scans were performed at 60°C/h between 15 and 50 °C for all samples.

The MicroCal software, provided with the calorimeter, was used to correct the thermogram baselines and to subsequently measure the transition temperatures at the peak maximum, the widths at half-height and the enthalpies from the area under the thermogram peak.

2.8. Coarse-grained Molecular Dynamics Simulations (CG-MDS):

All simulations were performed using the GROMACS 5.1.4 program package [36], [37] and MARTINI 2 coarse grain forcefield [38]. Fully hydrated 9:1 mole ratio bilayers (POPC:SAPC; POPC:SDhaPC; POPC:SDpaPC; POPC:DSPC) and pure POPC bilayer were constructed using the bilayer builder *insane* [39]. Coarse grain models of phospholipids are available on the web portal cgmartini.nl.

For SDpaPC lipid, we used the same bonded parameters from existing lipid, adapting some beads and mapping a new lipid (18:0; 22:5 n-3) to distinguish the ω3-PUFAs 18:0 22:5 and the ω6-PUFAs 18:0 22:5.

The systems were hydrated using the standard water model in Martini. A physiological concentration of 150 mM of NaCl was also included in the systems to match physiological conditions. For all simulations a box of 18 × 18 × 9 nm^3 was used. Each system was energy-minimized (steepest descent, 15000 steps) and simulated for 0.5 ns using a short time step of 10 fs to relax the membrane area, followed by production runs using a time step of 20 fs.

The simulations were run in the isothermal-isobaric ensemble, at 310 K and 1 bar. The temperature was controlled using the V-rescale thermostat [40] with a coupling constant of τ_T = 1.0 ps. The pressure was controlled with a Parrinello-Rahman barostat [41] at a pressure

of 1 bar (semi-isotropic coupling) using a coupling constant of $\tau p = 12.0$ ps and a compressibility of $\beta = 3 \times 10^{-4}$ bar^{-1}.

Reaction-field method with a cutoff of 1.1 nm in conjunction with a dielectric constant of 15 was used to model the electrostatic interactions. The Van der Waals interactions were calculated using a cut-off schema, with a cut off of 1.1 nm and were modified using potential shift verlet. The analyses were performed using tools available on the martini web portal cgmartini.nl (do_order_multi.py; do_order_gmx5.py) and using GROMACS tools. The lipids are all randomly distributed in the beginning of the simulation.

Values of mean and Gaussian curvature were averaged over all the frames of the trajectory to get a general overview of the impact of the lipid composition in term of polyunsaturation on the surface and membrane curvature.

3. Results

In an attempt to obtain the maximum information possible on the impact of PUFAs on membrane properties, PUFAs of both ω3 and ω6 type (thus that differ by the position of the first double bond relative to the terminal methyl) and possessing a varying number of double bonds were employed in this study. To enlarge the type of investigated PUFAs and since not all PUFAs combinations are commercially available, experiments were run on both cells enriched with free PUFAs, and lipid model systems composed of phospholipids containing polyunsaturated fatty acid chains (PUFA-PL) (Table I). Below, we briefly detail which systems were used in which type of experimental and/or theoretical studies.

In terms of PUFAs, cells were treated with: DHA, AA, DPA-ω3 and DPA-ω6. Such PUFA-enriched cells were used to investigate PUFAs impact in cell morphology and elasticity by AFM (section 3.2.1) and fluidity by Laurdan fluorescence (section 3.2.2). *As per* the phospholipids used for experimental studies, POPC (16:0-18:1) was used as a major component of cellular membranes and non-polyunsaturated phospholipid.

Cholesterol was also included to contribute to a certain rigidity as usually observed in cellular membranes. PUFA-PLs used were: SAPC (18:0-20:4; an ω6 with 4 unsaturations) and SDhaPC (18:0-22:6; an ω3 with 6 unsaturations). DPPC (16:0-16:0) and DSPC (18:0-18:0) were used as saturated phospholipids.

For modeling studies, in addition to POPC, cholesterol, SAPC and SDhaPC, SDpaPC (18:0-22:5; 5 unsaturations) was used. Of note, while SDpaPC could be presented in the ω3 and ω6 versions, due to the simplification in Coarse-Grained Molecular Simulations where a single

bead stands for three independent atoms, the ω3 and ω6 versions of SDpaPC could not be distinguished in our hands.

Table I. List of the polyunsaturated fatty acids (PUFAs) and phospholipids containing polyunsaturated fatty acid chains (PUFA-PLs) used in this study.

Shorthands	Structure	Abbreviations
C20:4, n-6	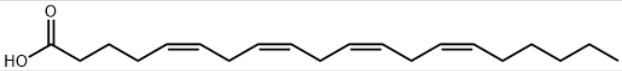	AA
C22:5, n-6	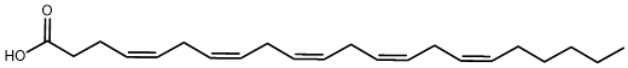	DPA-ω6
C22:5, n-3	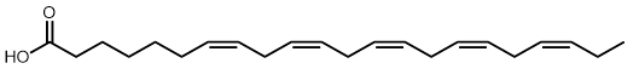	DPA-ω3
C22:6, n-3	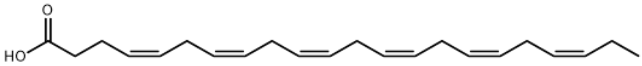	DHA
PC 16:0 ; 18:1 n-9	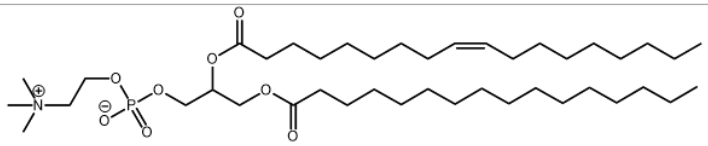	POPC
PC 18:0 ; 20:4 n-6	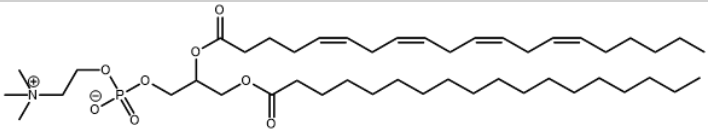	SAPC
PC 18:0 ; 22:6 n-3	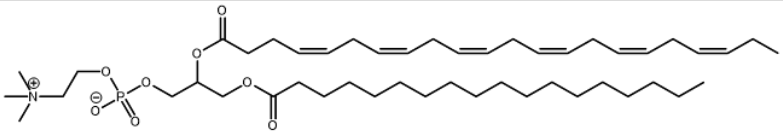	SDhaPC
PC 18:0 ; 22:5 n-3	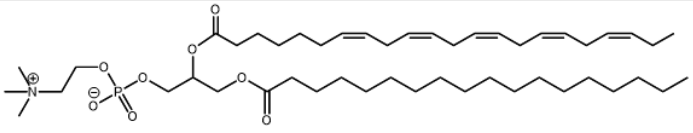	SDpaPC
PC 18:0 ; 18:0	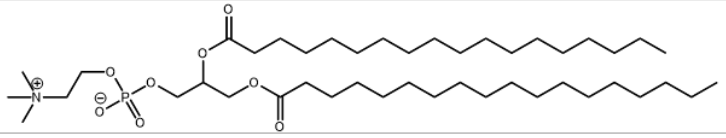	DSPC
PC 16:0 ; 16:0	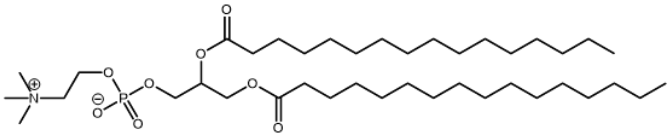	DPPC

3.1. PUFA cellular membrane enrichment

Lipidomic analysis performed in total cell membranes have previously revealed the efficient incorporation of DHA, DPA and AA [42] in cell membranes, up to a 10% enrichment-level. However, the precise cellular location of those PUFAs remains elusive. Here, we have used Confocal Raman spectroscopy to localize the accumulation of the only commercially available modified PUFA compatible with Raman detection, the DHA-alkyne inserted in HEK cells. It must be noticed that PUFA-alkyne cell treatment perturbs cell viability and that the data shown below correspond to experiments where cells were less affected.

The Raman spectrum of unsaturated fatty acids presents several specific bands: an intense band at 1661 cm^{-1} assigned to the νC=C vibrational mode and a band at 3018 cm^{-1} assigned to νCH (=C-H) vibrational mode [43]–[45]. However, those bands all are superimposed to other cell-specific signals and cannot be detected at low concentration such as the lipid enrichment performed here. To circumvent this, we used DHA labeled with a Raman tag whose signal arise in the silent region (1800-2600 cm-1) of the cellular Raman spectrum, so called because in this region no endogenous biological molecules display Raman signature, enabling detection of minute concentrations of labeled compounds. The labeling of the DHA by alkyne group is clearly identified on the Raman spectrum with a very intense band at 2099 cm^{-1} attributed to the νC≡C vibrational mode (Fig. S2, Supplementary Information). Figure 1A displays the Raman spectra of the control cell (black) and cell incubated with DHA-alkyne (red). Figure S3 shows the optical image of fixed cells. Both spectra exhibit similar broad bands assigned to vibrational modes of lipids, proteins (amide band + amino acids residues) and only the Raman spectrum of cells incubated with DHA-alkyne shows a band at 2099 cm^{-1} characteristic of the νC≡C vibrational mode. Figure 1B shows an optical image of fixed cells after incubation with labeled DHA and the corresponding Raman image based on the νC≡C band intensity is presented in Fig.1C. The superposition of the Raman and optical images (Fig. 1D) allows a

better assessment of the location of DHA-alkyne which is mostly observed in the plasma membrane with no evidence of accumulation in lipid bodies.

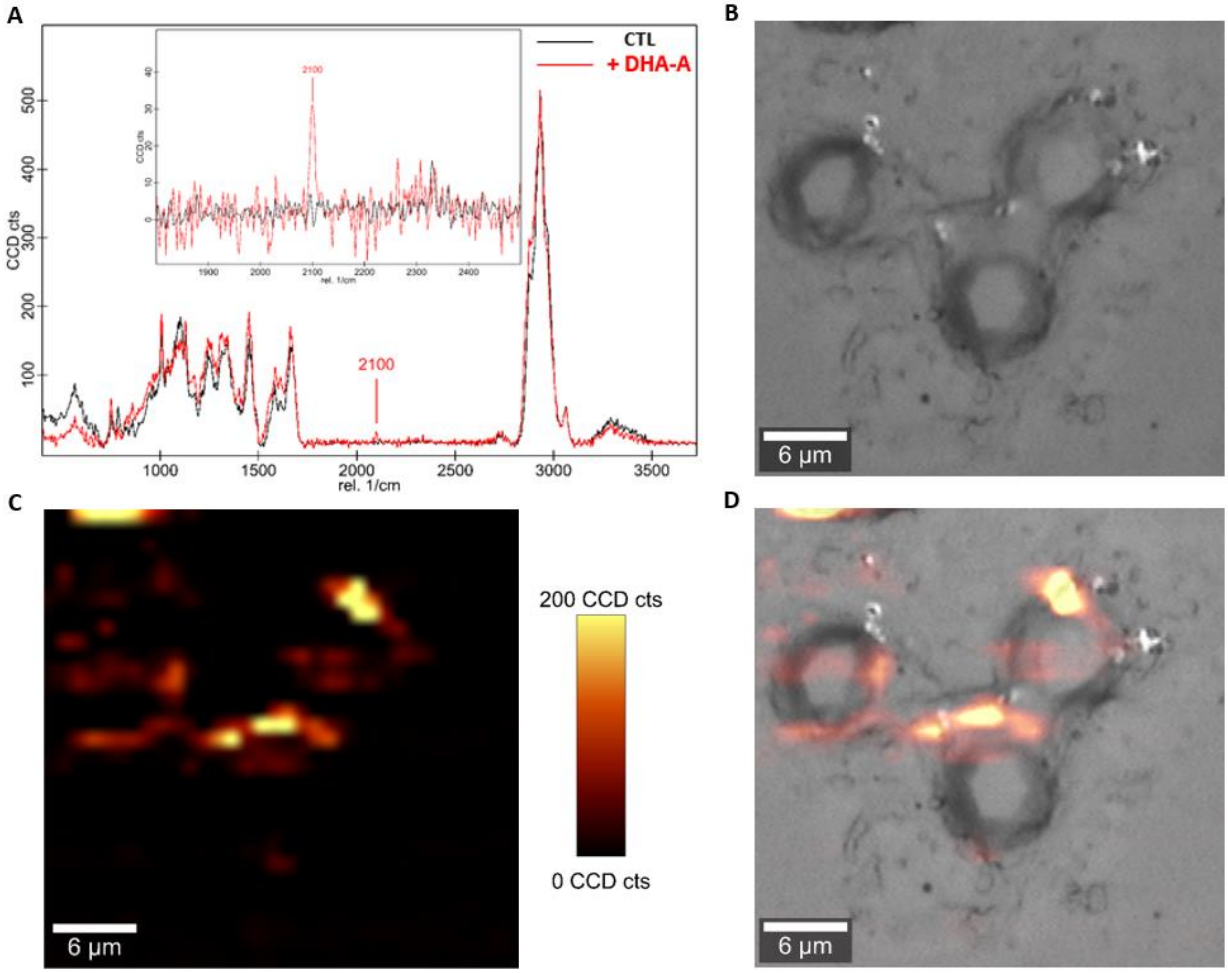

Figure 1. (A) Raman spectra of fixed non-treated (black) and incubated with DHA-alkyne HEK cells (red). The insert shows a zoom in the region of the νC≡C bond of the alkyne group. B) Optical image of fixed cells after incubation with DHA-Alkyne. C) Raman image of the integration of the C≡C stretching band at 2100 cm^{-1}. D) Superposition of optical (B) and Raman images (C).

3.2. PUFA impact in the lipid membrane physico-chemical and mechanical properties

3.2.1. Cell membrane morphology and elasticity

Given such a localization of PUFA, and the role of the plasma membrane in key cellular processes (*e.g.* adhesion, signalisation, morphogenesis), we then sought to explore their putative effect on the elastic and morphological behaviour of HEK enriched cells. Due to

straightforward sample preparation and the possibility of observing samples under near physiological conditions, AFM has emerged as a powerful tool to observe the morphology of cells and quantitatively measure their mechanical properties at the nanoscale [31], [46], [47].

Even, recent advances have pushed the technique forward, in the so-called multiparametric modes, allowing a simultaneous and quantitative mapping of cellular topography, elasticity, and viscosity at high resolution [27], [48].

Thus, to investigate whether cell enrichment in PUFA change cell morphology and elasticity, live cells were analyzed by AFM imaging in the PeakForce QNM multiparametric mode. Representative topographical images of control and PUFA-enriched HEK-293 cells are reported in Figure 2, with the corresponding mechanical properties maps.

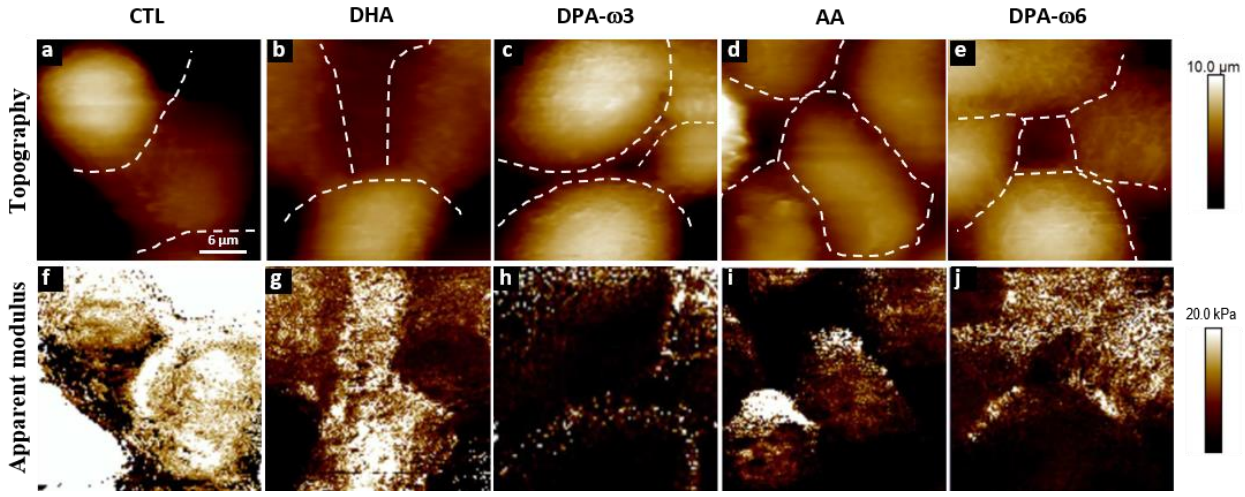

Figure 2. Topographical and mechanical maps of non-enriched (control cells, CTL) and PUFA-enriched HEK-293 cells. For each condition, i.e. HEK-293 control cell and cells enriched with DHA, DPA-ω3, AA, DPA-ω6, AFM topography images (a–e) and corresponding mechanical apparent Young's modulus maps (f–j) are shown. Dashed white lines on the AFM height images represent cell limits.

Untreated HEK cells and those enriched in PUFA feature similar round to elongated shapes, which might be somehow modified by the packing of several cells together. The height of the cells was ~ 8 µm, without any significant impact of PUFA enrichment. Qualitative comparison of the mechanical mapping of the cells (Fig. 2) shows a lower apparent Young's modulus for the PUFA-enriched cells compared to the control HEK-293 cells, as shown by mostly a darker contrast, suggesting those PUFA do have an impact on the membrane elasticity. Force distance curves recorded on the perinuclear area of the cells, to avoid any nucleus edge effect, then allowed us to quantitatively evaluate the mechanical properties (Young's modulus) of the cells (Fig. 3).

Given the heterogeneity of the cell structure, >1000 FD curves were recorded for each map and three areas over the cell were probed to account for the potential broad distribution of the Young's modulus (Fig. S1C, Supplementary Information).

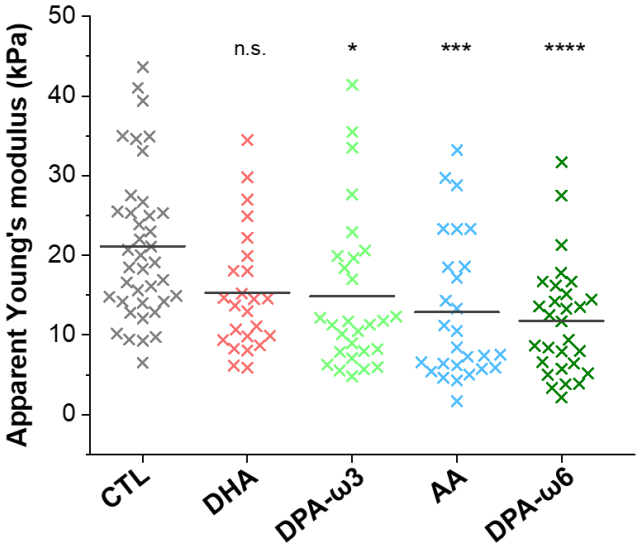

Figure 3. Elasticity data of non-enriched (control, CTL) and PUFA-enriched HEK-293 cells, showing the apparent Young's modulus (aYM) of cells (>24 cells; >1000 curves per cell). For each condition, data from three independent experiments is represented with each point representing the median aYM for one cell. Horizontal lines are the mean aYM for each condition. Statistical significance was assessed by a Kruskal-Wallis test with Dunn's multiple comparisons test, with n.s. = non significant, * $0.01 < p < 0.05$, *** $p < 0.005$, **** $p < 0.0001$.

Table II. Mean apparent Young's modulus and associated confidence intervals at 95% for non-enriched and PUFA-enriched HEK-293 cells.

	CTL	DHA	DPA-ω3	AA	DPA-ω6
Mean apparent Young's modulus (kPa)	21.12	15.33	14.86	12.88	11.75
Apparent Young's modulus (kPa) CI_{95}	[16.52, 22.20]	[11.16, 16.80]	[9.83, 15.65]	[7.57, 13.51]	[7.62, 12.50]

Though the aYM distribution follows a normal distribution (Fig.S1C), when considering a population of cells, whether non-enriched or enriched in PUFA, a lognormal distribution of the data was observed (Fig.3). Mean values and confidence intervals at 95%

were calculated and are displayed in Table II. HEK-293 control cells present a mean Young's modulus of 21.1 kPa with a confidence interval at 95% of [16.52, 22.20]. AFM data indicate that ω3 and ω6 PUFAs-enriched cells exhibited significantly lower Young's modulus in the range of DHA (27 % decrease compared to untreated cells) < DPA-ω3 (29%) < AA (39%) < DPA-ω6 (44%). Overall, the data indicate that PUFA-cell enrichment has pronounced effects on the elasticity properties of HEK-293 cells, depending on the nature of the PUFA. In fact, all PUFAs induce a softening of the cell membrane with a more pronounced impact of ω6 compared to ω3 PUFAs.

Noteworthy, these AFM nano-indentation experiments did not evidence any direct correlation between the number of double bonds (unsaturation level) and membrane elasticity, neither for ω3 nor for ω6, suggesting the essential role of the position of unsaturation beyond the number of unsaturation in cell elasticity.

3.2.2. Fluidity

The change in cell elasticity upon PUFA-enrichment might result from and/or induce *e.g.* a modification in membrane fluidity, two characteristics known to be co-dependent [49], [50].

To evaluate the impact of lipid unsaturation on membrane fluidity, the fluorescent probe Laurdan was used to determine GP, a parameter derived from the Laurdan emission spectrum, whose change reflects faithfully the change in fluidity during the gel-fluid transition of phospholipids [35]. GP values of PUFA-enriched cells (DHA, DPA-ω3; DPA-ω6, AA) were measured and compared to that of control cells. As shown in figure 4A, ω6-enriched cells (DPA-ω6, AA) exhibit the lowest GP values indicating significant higher membrane fluidity than control cells. On the opposite, no differences regarding membrane fluidity were detected between ω3-enriched cells (DHA, DPA-ω3) and control cells. Interestingly, DPA-ω6 and AA-enriched cells feature similar fluidity, higher than DHA and DPA-ω3-enriched cells both also showing similar GP values. Such results suggest that membrane fluidity depends more on the position of the first unsaturation from the methyl terminal group (i.e. ω6 vs ω3 PUFAs) than on the number of unsaturated bonds in the carbon chain. The importance of the first unsaturation is further supported by the higher membrane fluidity of DPA-ω6-enriched cells as compared to those enriched with DPA-ω3, those two PUFAs differing only by the position of the first unsaturation (see table I).

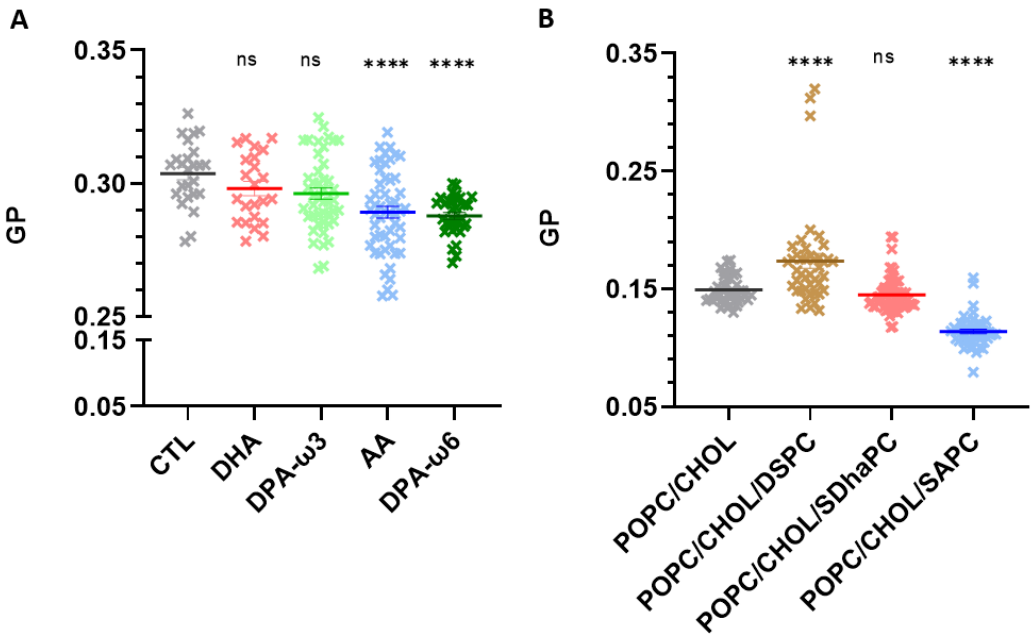

Figure 4. Membrane fluidity data showing the GP values observed in control and PUFA (DHA, DPA-ω3, AA, DPA-ω6)-enriched HEK-293 cells (A) or in MLVs composed of: POPC/chol (8/2 mol/mol), POPC/chol/DSPC, POPC/chol/SDhaPC, POPC/chol/SAPC (7/2/1 mol/mol/mol) (B). Data are expressed in terms of mean and associated standard error of mean (SEM) from three independent experiments with **** $p < 0.0001$, ns $p \geq 0.05$ by ordinary one-way ANOVA test with Dunnett's multiple comparisons test.

To further understand the effect of ω3 and ω6 PUFAs on membrane fluidity, we used lipid model systems (MLVs) composed of POPC and cholesterol in absence (POPC/cholesterol, POPC/chol/DSPC) and presence of ω3 or ω6 PUFA-PL (SDhaPC and SAPC respectively).

The results indicate membrane lipid fluidity to be more important in MLVs containing monounsaturated and polyunsaturated fatty acids (POPC/chol, POPC/chol/SDhaPC, POPC/chol/SAPC) than MLVs composed of a mixture of monounsaturated and saturated fatty acids (POPC/chol/DSPC) (Fig. 4B). In accordance to our previous results, MLVs containing ω6-PUFA are the ones with the lowest GP values reflecting a higher membrane fluidity.

3.3. Phase transition temperature

Membrane fluidity is obviously related to lipid phase transition and the temperature at which such transition occurs critically depends on lipid nature and intrinsic properties (*e.g.* length of fatty acid chain and degree of unsaturation) (for a review see [51]). We thus carried out a calorimetric study, using differential scanning microcalorimetry (DSC), to explore the effect of lipid polyunsaturation on the structure of biological membranes. We sought to

investigate the changes in the DPPC phase transition, allowed by its narrow thermal transition endotherm, upon interaction with free ω3 and ω6 fatty acids (10% mol), namely DHA, DPA-ω3, AA and DPA-ω6 (Fig. 5A). DPPC was chosen rather than POPC due to the fact that the phase transition of DPPC occurs above 0 which is not the case for POPC. Pure DPPC MLVs displays a pre-transition peak centred at 36.1°C, followed by the main rippled-to-liquid crystalline phase transition at 41.6°C in good agreement with reported values [51]. Qualitatively, as shown in the corresponding thermograms, treatment with all PUFAs, except DPA-ω6, downshifted the phase transition temperature of DPPC, caused a broadening of the DPPC main transition endotherm and the disappearance of the pre-transition peak. Main-transition temperatures (T_m) and enthalpies (ΔH) reflecting the fluidity of the membrane and widths at half-height ($T_{1/2}$) reflecting its cooperativity were calculated from three independent experiments (Table III). Except for DPA-ω6-containing mixtures, T_m decreased in the order of DHA~AA < DPA-ω3 and $T_{1/2}$ increased in the order of AA < DHA < DPA-ω3. The data indicates that these three fatty acids, despite subtle differences, preferentially partition to the fluid rather than the solid lipid phase MLVs and induce a lower cooperativity in the melting process. Such decrease in Tm corresponds to an increase in fluidity at temperatures slightly smaller than the Tm of the membrane in the absence of the PUFA-PLs.

Overall, the inclusion of either free PUFAs resulted in endotherms that are more asymmetric that that of DPPC alone. This suggests that the inclusion of free PUFAs results in non-ideal mixing of the lipid components with domains containing higher content of free PUFAs and other domains with lower [51], [52]. DPA-ω6-containing mixtures revealed an intriguing and somehow counterintuitive behaviour with a thermogram and energetic properties similar to pure DPPC (Fig. 5, Table III).

Given the impact of DPA-ω3 on the structural properties of DPPC membranes, these results demonstrate the key role of the unsaturation position in the interaction of PUFAs with saturated phosphatidylcholines. Still, the fluidifying effects of ω6 AA (opposite to DPA-ω6) and both ω3 PUFAs, DHA and DPA-ω3, additionally argue in favour of a strong interplay between the number of unsaturations and their positions when interacting with DPPC MLVs.

We then wondered if direct incorporation of lipids with polyunsaturated PUFA acyl chains would induce similar changes in PC membranes as free fatty acids. SAPC and SDhaPC were chosen to mimic the behaviour of ω3 DHA and ω6 AA fatty acids respectively. SAPC and SDhaPC, to a larger extent, both broadened and shifted the phase transitions of DPPC MLVs to a lower temperature (Fig. 5B) with its pre-transition no longer observable. Such

results, highlighting a fluidification of the DPPC membrane, at temperature below the *Tm* of the pure lipid, when including higher proportion of polyunsaturated acyl chains, are consistent with those reported for free PUFAs. Besides, they also suggest a higher impact of SAPC as compared to SDhaPC on the physical properties of the membrane. Yet, both the chain length and number of unsaturations in SAPC and SDhaPC differ preventing a strict conclusion on the sole role of the unsaturation position (ω3 *vs.* ω6).

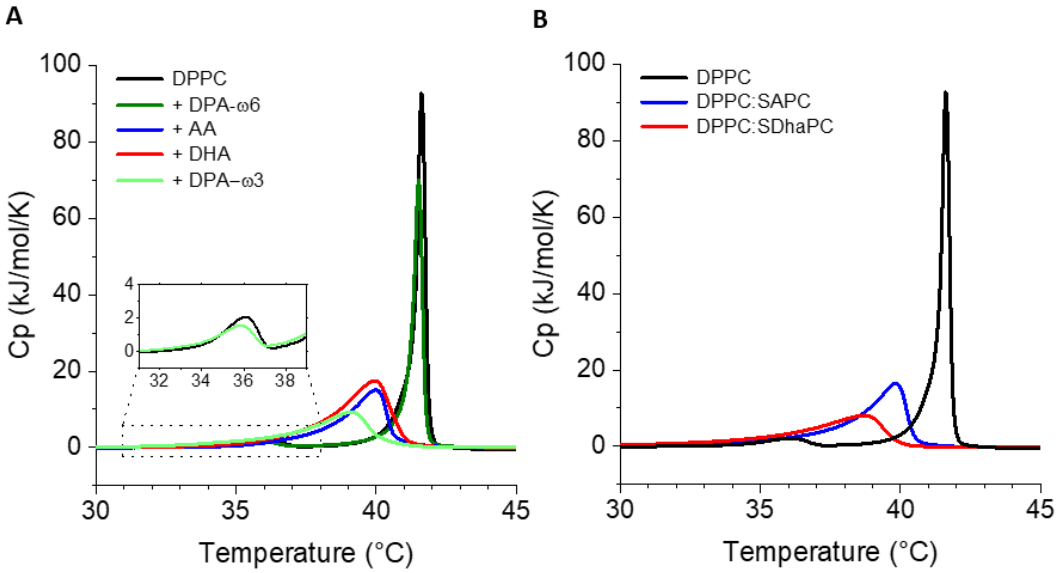

Figure 5. Differential scanning calorimetry thermograms of MLVs composed of DPPC alone or with 10 mol% free PUFAs, either ω3 (DHA, DPA-ω3; blue) or ω6 (AA, DPA-ω6; red) (A) and of DPPC alone or with 10 mol% of PUFA-PLs (SAPC, SDhaPC) (B). Zoom in Panel A depicts the pre-transition.

Table III. Thermodynamic properties for phase transitions of unsaturated phospholipid MLVs, obtained either by treatment with free fatty acids or by incorporation of lipids with PUFA chains (*).

	Number of unsaturations	Unsaturation position	T_m (°C)	$T_{1/2}$ (°C)	ΔH (kJ/mol)
DPPC	0	-	41.57 ± 0.05	0.33 ± 0.02	45.56 ± 3.57
+ DHA	6	ω3	39.99 ± 0.05	1.90 ± 0.17	46.21 ± 0.34
+ DPA-ω3	5		39.16 ± 0.04	2.33 ± 0.09	30.67 ± 0.68
+ SAPC*	4		39.71 ± 0.11	1.98 ± 0.28	37.46 ± 1.24
+ AA	4	ω6	40.04 ± 0.06	1.62 ± 0.04	33.26 ± 0.97
+ DPA-ω6	5		41.55 ± 0.03	0.33 ± 0.03	38.47 ± 0.30
+ SDhaPC*	6		38.71 ± 0.02	2.85 ± 0.22	29.13 ± 1.50

3.2.4. Thickness

Laurdan and DSC experiments presented above unambiguously demonstrated the PUFA-dependent fluidity of the cell membrane. Such fluidification might result from a loosed packing of lipids within the membrane (increased lipid area, as further discussed in the discussion section), and might then translate into a change in membrane thickness. To tackle this hypothesis, CG-MDS was used. Lipid membranes composed of POPC and a PUFA-PL in absence (POPC/PUFA-PL; 9/1 mol/mol) and presence of cholesterol (POPC/Chol/PUFA-PL; 7/2/1 mol/mol/mol) were modeled for 10 μsec at 37°C (further experimental details to be found in section 2.8). The distance between the phospholipid headgroups of different phospholipid species present in each leaflet were measured for 3 independent replicas.

The thickness of the bilayer was highly impacted by the presence of PUFA-PLs both in absence and presence of cholesterol. On one hand, in absence of cholesterol, a direct correlation was observed between the number of unsaturations in the phospholipid fatty acid chain and the lipid membrane thickness. Phospholipid membranes containing PUFA chains are thinner by about 1 Å relative to a pure POPC membrane (Fig. 6A). On the other hand, phospholipid mixtures containing cholesterol also showed a decrease in thickness when PUFAs chains were included in the mixtures (Fig. 6B), but no direct correlation was observed between thickness and level of lipid unsaturation. Of note, and consistently with literature, lipid mixtures containing cholesterol, either in presence or absence of PUFA, showed overall a higher thickness (~1 Å) than POPC-membranes.

Altogether, these simulations highlight the thinning effect of PUFAs on model membranes, correlating well with their influence on membrane fluidity described above.

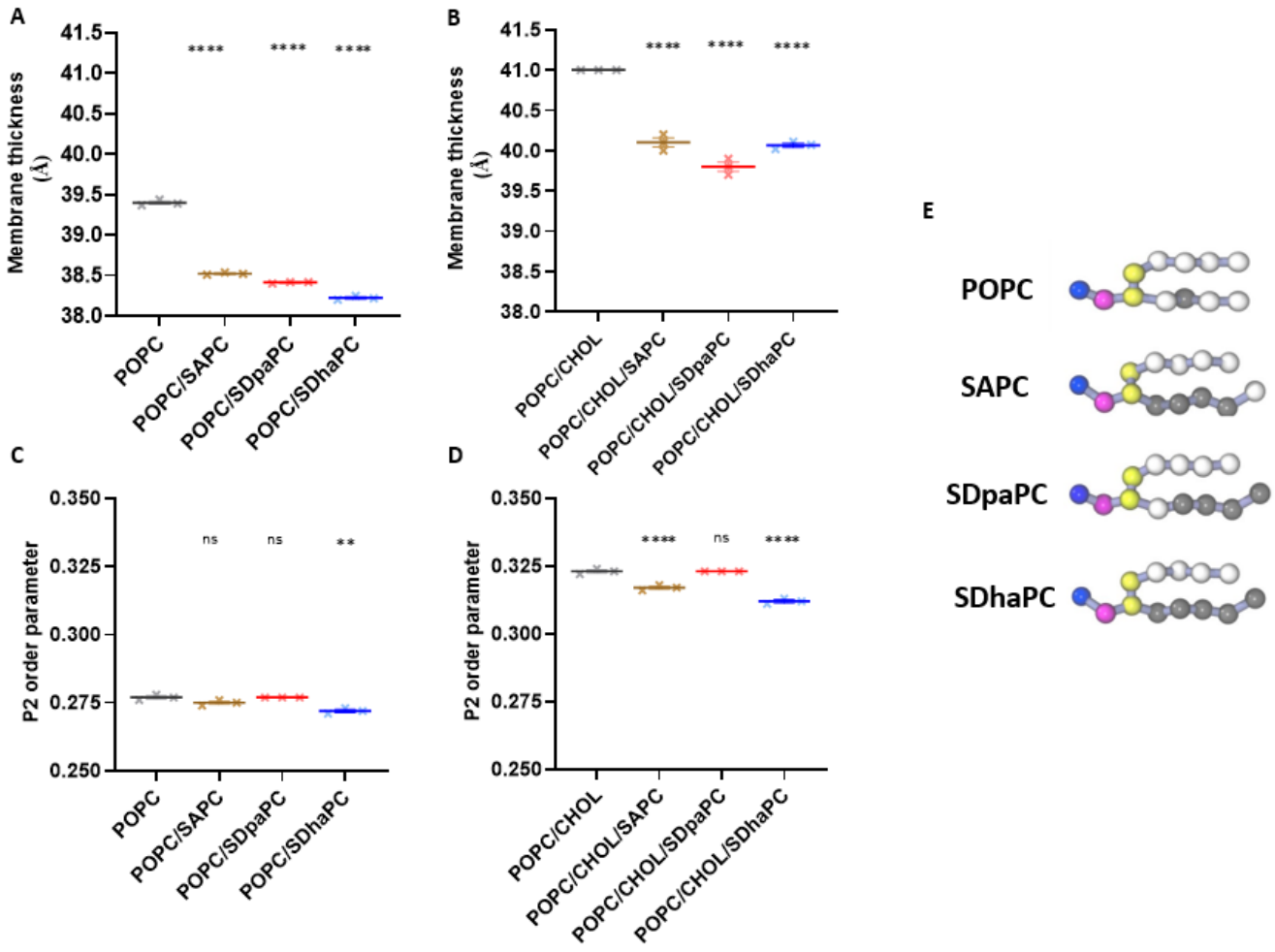

Figure 6. Lipid membrane thickness (A, B) and average order parameter P2 (C, D) of POPC-mixtures or POPC/PUFA-PL mixtures in absence (POPC/PUFA-PL; 9/1 mol/mol) (A, C) and presence (B, D) of cholesterol (POPC/Chol/PUFA-PL; 7/2/1 mol/mol/mol). E) Phospholipid representation in beads for CG-MDS with blue corresponding the choline (NC3), pink to phosphate (PO4), yellow glycerol (GL) and gray to the fatty acid chain with dark ones corresponding to double and light ones to single bonds. Data are expressed in terms of mean and associated standard error of mean (SEM) from three independent experiments with ns $p \geq 0.05$, ** $p < 0.01$, **** $p < 0.0001$ by ordinary one-way ANOVA test with Dunnett's multiple comparisons.

3.2.5. Order parameter

Given the significant impact of PUFA levels on membrane thickness and the correlation between thickness and membrane order parameter, we then investigated PUFA effect in this later property by CG-MDS. The lipid order parameter is defined as: $P_2 = 0.5 \times (3\cos^2\theta - 1)$, where θ is the angle between the direction of the bond formed by two coarse-grained beads and the bilayer normal. A P2 value of 1 corresponds to perfect alignment, $P_2 = -0.5$ to perfect antialignment, and P2 = 0 to a random orientation of molecules with respect to the bilayer normal [53]–[55]. The order parameter was calculated by averaging all lipid tails and over last 2 μs in the simulations. CG-MDS data clearly indicate that the presence of PUFA-PLs impacts the average ordering of the POPC alkyl chain (Fig. 6C, D). Overall, the data shows no direct correlation between the number of unsaturation and the order parameter. It seems that the position of the unsaturation is important as having unsaturated bonds in the polyunsaturated chains that are localized at about the same level as the double bond of POPC impacts order parameter. Indeed, the presence of a double bond in position 3 (right below the phospholipid headgroup; which is the case for SDhaPC) results in a higher impact in the POPC order parameter.

Overall, the same tendency is observed, in terms of polyunsaturation impact in order parameter, in absence and presence of cholesterol, although more marked in its presence (higher P2 values). This is expected since the presence of cholesterol is known to increase membrane ordering [56].

3.2.6. Membrane curvature

Considering the thinning and fluidifying effects of PUFA on cell membranes, we finally sought to investigate its role in membrane curvature. Compared to pure POPC, in which there is only one unsaturation in *cis* conformation, polyunsaturated chains can adopt multiple conformations, due to several unsaturations in *cis* conformation and the rotatable simple bonds present between them. In this study, we calculated mean and Gaussian curvature of pure POPC lipid bilayer, and of mixtures containing PUFA-PLs SAPC, SDhaPC and SDpaPC respectively from CG-MDS using MDAnalysis MembraneCurvature realized by Estefania Barreto-Ojeda from Calgary University [57]**.** The mean curvature calculates the arithmetic mean of two principal curvatures and the Gaussian curvature calculates the geometric mean of the two principal curvatures.

The results presented in Fig. 7 of the curvature calculation correspond to the last 20 ns of the 10 μs simulation. The calculation was carried out along the last microseconds at multiple

times. In the absence of notable changes, only the graphs corresponding to the last 20 ns are presented. Typically, in lipid bilayers phospholipid headgroups are the most straightforward atoms of reference from which to derive surfaces.

Thus, we have chosen phospholipid headgroups of phosphate beads of all the lipids in the simulation box for surface studies. In the Martini representation, these beads are called PO_4. First, in all systems, whatever the PUFA content, obtained lipid bilayers positive-curvature (red) and negative-curvature regions (blue) are superimposed, in both the upper and lower leaflets. Second, while negative mean curvature dominates in the central region of the pure POPC bilayer, mixtures containing PUFA exhibit a clear domain of positive mean curvature, either in the center of the two leaflets for POPC/SDhaPC or along the y-axis for POPC/SAPC and POPC/SDpaPC. Finally, as opposed to POPC bilayer where regions of negative Gaussian curvature dominate in both leaflets, mixtures with PUFA-PLs also feature regions of positive Gaussian curvature. Strikingly, those results emphasize that, in the pure POPC bilayer and in mixtures with saturated lipids, negative Gaussian regions present saddles in the bilayers while in presence of PUFA-PLs, the membrane displays local concave regions (green colored regions). This can be translated to the high flexibility of the membrane revealed during the simulation, in good agreement with previous studies. Indeed, as reported by Pinot *et al* [58], PUFA-PLs decrease membrane-bending rigidity and more generally their flexibility along the membrane normal (z direction) which might soften various mechanical stresses in the membrane [59].

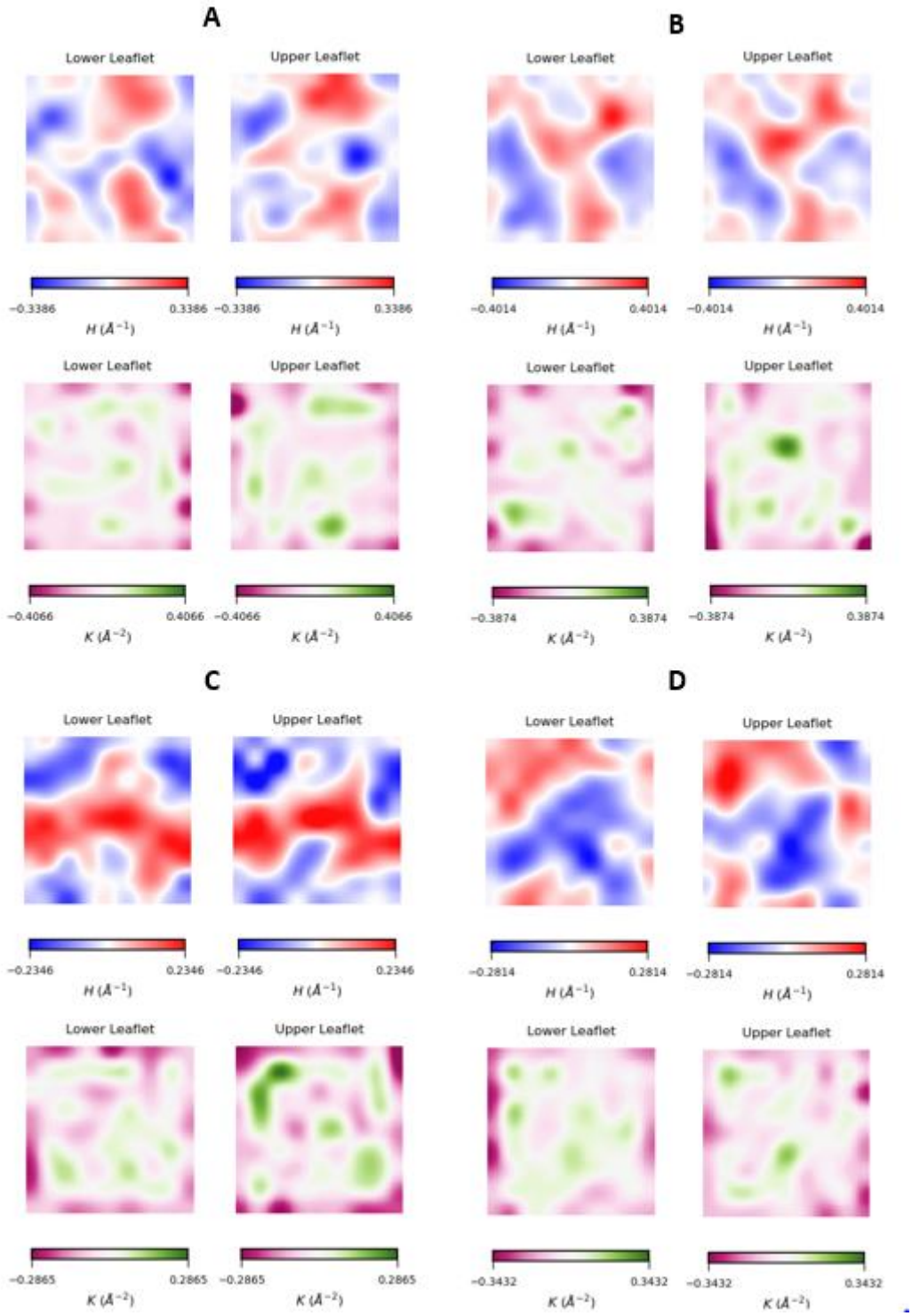

Figure 7. Contour plots of Mean (upper panels) and Gaussian (lower panels) membrane curvature of the lower and upper leaflet obtained by CG-MS during a 10 μs simulation of POPC (A), POPC/SDhaPC (B), POPC/SAPC (C), POPC/DpaPC (D) (9/1 mol/mol). Mean curvature (H) gives information about the "inverted shape" of the surface. Positive mean curvature indicates valleys (red), negative mean curvature indicates peaks (blue). Gaussian curvature (K)

is associated to the elasticity of the membrane, negative Gaussian curvature represents saddles (pink), positive Gaussian curvature represents concave regions (green).

4. Discussion:

PUFAs, often taken as dietary supplements, have been associated with health benefits in diverse pathologies, such as neuronal disorders and cardiovascular diseases. They are thus seen as potential complements in therapeutic practices to improve, for instance, psychiatric symptoms of patients with schizophrenia some of whom exhibiting a constitutive or acquired PUFA deficiency [60], [61].

For such strategy to be efficient, and in turn promoted, we first need a comprehensive understanding of the underlying mechanisms of PUFAs roles within cells. Interestingly, PUFAs are known to be directly or indirectly involved in diverse cellular processes, related to neuropathologies, *e.g.* SNARE assembly [62], recycling of synaptic vesicles [63], [64], and modulation of specific protein activities such as rhodopsin and protein kinase C [65]. Those roles not only rely on the conformational flexibility of PUFAs to assist the dynamics of membrane protein conformational changes [20], [66] but also on their ability to first modulate membrane properties, which remains so far elusive.

Here, we thus aimed at deciphering the impact of PUFAs in the physical and mechanical properties of lipid membranes, essential in subsequent cellular functions, *e.g.* elasticity, fluidity, phase transition temperature, thickness, order and curvature. To obtain the most complete possible analysis of lipid polyunsaturation in such properties, we have combined *in cellulo* and *in vitro* approaches, respectively with PUFA-enriched cells and lipid models systems containing different PUFA-PLs. Besides, to account for the wide diversity of PUFAs, variations of those membrane properties were investigated upon treatment with PUFAs and PUFA-PLs harboring different number of double bonds and differing in the location of their first double bond (ω3 and ω6). Importantly, previous studies [42] have demonstrated that the incubation of cells with PUFAs allows for their incorporation into cellular membranes, mostly in PC and PE, with a 5-10% enrichment level closely resembling the deficiency levels observed in patients suffering from psychiatric disorders [67]. By means of Raman imaging, we here further revealed that PUFA only accumulate in the plasma membrane, rather than in other intracellular organelles membrane. Consequently, to allow a comprehensive comparison with cellular systems, we here only investigate model systems containing 10% PUFA-PLs.

Our AFM experiments first reveal subtle but significant increase in cell elasticity (as shown by the decrease in Young's modulus) upon incorporation of PUFAs in cell membranes (Fig. 3). These results are reinforced by our molecular simulations on simplified lipid bilayers showing higher and more heterogenous curvature for PUFAs-enriched membranes (Fig.7), suggesting their higher flexibility and deformability. Such behavior is in agreement with previous studies highlighting the higher flexibility or bending elasticity of giant unilamellar vesicles (GUV) containing PUFA [58], [68], [69], [70]. Pinot and coworkers have attributed this behavior to the ability of SDhaPC (C18:0-C22:6, n-3) to reduce packing defects in POPC-GUV upon bending, the PUFA enriched-membrane becoming more amenable to deformation by a pulling force [58], in turn favoring endocytosis (membrane fission by endophilin and dynamin). Similarly, using the micropipette pressurization approach, the Evans group reported that GUV containing PUFA-PLs with 2 to 6 double bonds experienced a drastic decrease in their bending stiffness [68]. Interestingly, both these studies also highlight the impact of the degree of unsaturation in membrane flexibility which is not that straightforward in our AFM experiments likely due the systems investigated (models *vs.* cells respectively) and the amounts of PUFA-PLs used (up to 100% *vs.* 10% respectively.). Strikingly, our data additionally reveals that ω6 PUFA-enriched cells are significantly more elastic than ω3 PUFA-enriched cells. It is thus interesting to note that cell membrane elasticity, contrarily to what one could expect, is not proportionally related to the degree of lipid polyunsaturation in the membrane but rather influenced by the position of double bonds, the impact being higher when the double bonds are closer to the lipid headgroup region. As membrane ordering parameter increases along the fatty acid chain when going from the terminal methyl group to the headgroup region, the insertion of double bonds in closer proximity of this region is indeed expected to have higher impact in membrane elasticity.

Regarding membrane ordering, increase in lipid polyunsaturation, by means of free PUFAs addition in model membranes, has been shown to decrease the ordering of membranes [22], [65]. While our MD studies were performed with PUFA-PLs rather than free PUFAs and that we have followed the order parameter of POPC rather than that of fully saturated phospholipids like DPPC, we observe the same tendency. Our data agrees with the decreased order parameter observed by Hyvonen *et al* when going from a phospholipid containing 1 to 4 double bonds (in their case they have compared POPC with PAPC (1-palmitoyl-2-linoleoyl-*sn*-glycero-3-phosphatidylcholine) rather than SAPC, still the same unsaturated fatty acid chain as herein) [71]. There has not been a systematic study of the order parameter changes induced by the presence of PUFA-PLs of varying number and position of double bonds. Interestingly, our

results pointed that both the position and degree of unsaturation, even in a co-dependent manner, seem key in modulating membrane ordering. A maximal effect is observed in presence of cholesterol, explained by the fact that cholesterol, while increasing membrane ordering, also potentially maximizes the disordering impact of PUFA-PLs.

Variations in membrane elasticity upon PUFA-PL incorporation might result in membrane thickness changes, as shown by our CG-MS analysis on model systems. Indeed, those simulations indicate that the inclusion of PUFA-PLs in membranes leads to a reduction in membrane thickness of about 0.1 nm, without any significant different behavior between ω3 and ω6-PUFA-PLs. Noteworthy, in absence of cholesterol (POPC/PUFA-PL, 9/1 mol/mol), this decrease in thickness is very significant and directly correlated to the number of double bonds in the membrane, the thinner membrane being that containing SDhaPC (6 unsaturations, ω3). The decrease in membrane thickness comes as a consequence of the increased area per lipid, a key effect of unsaturation as reported [65], [72]. In the presence of cholesterol, this relationship is no longer observed, the thinner membrane being that containing DPA-ω3 (5 unsaturations, ω3). Those results highlight the increased level of complexity brought by cholesterol in the membrane, consistent with the different partitioning of specific PUFAs into cholesterol-rich domains [22]. The observed 0.1 nm-increase in membrane thickness is in good agreement with the one observed by X-ray diffraction studies [68] after introduction of a C18 with 2 versus 3 double bonds (0.06 nm), minor differences likely resulting from the amount of PUFAs, *i.e.* 10% in our experiments *vs.* 100% in this report. Of interest, the impact of lipid polyunsaturation in membrane thickness is also modulated by temperature and lipid phase. Simulations being performed at 310 K, temperature at which membranes are fluid, the thickness of the hydrophobic core of SDhaPC bilayers does not exceed that of POPC.

Furthermore, it has often been intuitively, yet erroneously, assumed that increasing fatty acid unsaturation would proportionally increase membrane fluidity [6], [21]. Actually, and paradoxically, previous studies have reported either an increased or an unchanged membrane fluidity upon increasing lipid polyunsaturation likely due to the distinct lipid environment of cellular and model systems therein used, which cannot be strictly compared. Indeed, cellular membranes are already naturally rich in unsaturated fatty acids so additional increments of unsaturation may result in very subtle changes while, in model systems, and depending on the chosen phospholipid mixture, the effects can be boosted. In addition, the natural cellular homeostasis of mammalian membranes can counteract dietary lipid perturbations and thus PUFA cellular enrichment can be rapidly compensated by upregulation of saturated lipids and

cholesterol [73]. Third, different PUFAs or PUFA-PLs partition differently in cholesterol rich domains (so-called rafts), inherently present in cellular systems but not always taken into account in model systems.

Jacobs and collaborators have notably reported the distinct behavior of two ω3-PUFA: while DHA tends to remain outside of rafts thus strengthening their formation, EPA partitions into rafts and tends to disorganize them [19]. In a global approach, investigating both PUFA-enriched cells and lipid vesicles containing PUFA-PLs (SAPC, SDhaPC), in absence or presence of cholesterol, we demonstrated an overall increased membrane fluidity, yet subtle, in the presence of lipid polyunsaturation without direct correlation with the number of unsaturations. Interestingly, as observed for cell elasticity, in both cellular and model systems, the impact becomes more pronounced and therefore significant for ω6 PUFA relative to ω3, suggesting that the closer the double bonds are from the headgroup region the higher the impact in the membrane properties.

Membrane fluidity is usually correlated with phase transition temperature of lipids, namely the gel to crystalline phase transition (T_m). Our calorimetric experiments showed a decreased T_m and decreased enthalpy and cooperativity of this transition upon inclusion of PUFA-PLs in the membrane, illustrating a reduction in intra- and inter-molecular van des Waal's interactions as previously reported (as example, [6], [21], [65], [74]). Indeed, unlike saturated phospholipid membranes where the acyl chains pack near uniformly in all-*trans* configuration in the gel state, in membranes containing PUFA-PLs, the lipid packing is distorted by steric restrictions associated with the presence of multiple rigid double bonds. While the introduction of the first and the second double bond in fatty acids changes dramatically the T_m and enthalpy of lipid phase transition, this is not the case for additional ones, where in certain cases only a slight increase has actually been observed [65], [74]. While in the case of PUFA-PLs, the decrease in T_m could be correlated to the number of double bonds (the decrease being lower for SDPC than SAPC), this could also be due to the position of the first double bond that differs between them. This hypothesis is further reinforced by the data obtained with free PUFAs, showing different thermodynamic properties between ω3 and ω6 DPA- (more impacted in the case of DPA-ω3). The key role of the unsaturation position has been earlier reported by Stubbs and Smith who have systematically changed the position of a double bond along the fatty acid chain, and revealed the highest impact in phase transition temperature with the double bond positioned in the middle of the fatty acid chain [6]. Yet, another systematic study by Wang and collaborators using 15 synthetic molecular species of

phosphatidylethanolamine (PE) with *sn-1* C_{20}-saturated and *sn-2* C_{20}-unsaturated fatty acid chains have reported the *Tm* to depend not only on the number but also on the position of the double bond [75].

The present work contributes to the understanding on how polyunsaturation in lipid membranes impacts the membrane physical and mechanical properties, crucial in diverse cellular processes and pathologies. While some properties seem to directly correlate with the number of double bonds present, *e.g.* membrane thickness, this is not at all a generality despite acknowledged, and intuitive, paradigm. Strikingly, the position of the first double bond in the chain also appears as a key criterion in regard to some membrane properties, as membrane elasticity and fluidity.

Unravelling membrane polyunsaturation effects on the physico-chemical properties of cell membranes is highly relevant in the context of psychiatric disorders, in which a considerable decrease in PUFA-PLs (specially of the ω3 type) is observed in the brain of a subgroup of usually more severe patients [11]–[17]. By altering the membrane physico-chemical properties, polyunsaturation can modulate the pharmacology of membrane receptors. Indeed, current studies by our team on PUFA-enriched cells have revealed PUFAs to function as allosteric modulators of the Dopamine D2 receptor, one of the major targets of antipsychotic (AP) drugs [42]. Moreover, membrane unsaturation can directly modulate the interaction of AP with the receptor. Indeed, as recently evidenced by Lolicato *et al* , ligands have shown to access a Dopamine receptor target (D3 in this study) by a two-step pathway the first consisting in their partition in the lipid membrane, and the second accessing the receptor laterally via the hydrophobic part of the transmembrane helices [76]. Therefore, one could postulate that the PUFA-induced alterations in membrane properties, revealed in our study, might impact GPCR signaling by modulating ligand accessibility to the receptor via this lipid pathway, energetically favorable.

Acknowledgements

PN would like to thank the Fondation de France and the Fondation Pierre Ouriez for supporting this fundamental work, which is preliminary to a better understanding of the non-direct receptor-related therapeutic properties of antipsychotics. The authors thank Malvern for providing a DSC instrument to perform the DSC experiments and for technical support on instrument use to Aymeric Audfray.

This study has received financial support from the French State in the framework of the Investments for the Future programme IdEx université de Bordeaux (a professor visiting scholarship provided to Galya Staneva).

References

[1] J. R. Marszalek and H. F. Lodish, "Docosahexaenoic acid, fatty acid-interacting proteins, and neuronal function: breastmilk and fish are good for you," *Annu. Rev. Cell Dev. Biol.*, vol. 21, no. 1, pp. 633–657, Nov. 2005.

[2] S. Takamori *et al.*, "Molecular Anatomy of a Trafficking Organelle," *Cell*, vol. 127, no. 4, pp. 831–846, Nov. 2006.

[3] T. Harayama and T. Shimizu, "Roles of polyunsaturated fatty acids, from mediators to membranes," *J. Lipid Res.*, vol. 61, no. 8, pp. 1150–1160, Aug. 2020.

[4] D. R. Robinson, L. L. Xu, C. T. Knoell, S. Tateno, and W. Olesiak, "Modification of spleen phospholipid fatty acid composition by dietary fish oil and by n-3 fatty acid ethyl esters.," *J. Lipid Res.*, vol. 34, no. 8, pp. 1423–34, Aug. 1993.

[5] H. R. Knapp, F. Hullin, and N. Salem, "Asymmetric incorporation of dietary n-3 fatty acids into membrane aminophospholipids of human erythrocytes.," *J. Lipid Res.*, vol. 35, no. 7, pp. 1283–91, Jul. 1994.

[6] C. D. Stubbs and A. D. Smith, "The modification of mammalian membrane polyunsaturated fatty acid composition in relation to membrane fluidity and function," *Biochim. Biophys. Acta - Rev. Biomembr.*, vol. 779, no. 1, pp. 89–137, Jan. 1984.

[7] V. Vásquez, M. Krieg, D. Lockhead, and M. B. Goodman, "Phospholipids that Contain Polyunsaturated Fatty Acids Enhance Neuronal Cell Mechanics and Touch Sensation," *Cell Rep.*, vol. 6, no. 1, pp. 70–80, Jan. 2014.

[8] Y. Du, C. G. Taylor, and P. Zahradka, "Modulation of endothelial cell responses and vascular function by dietary fatty acids," *Nutr. Rev.*, vol. 77, no. 9, pp. 614–629, Sep. 2019.

[9] D. S. Siscovick *et al.*, “Omega-3 Polyunsaturated Fatty Acid (Fish Oil) Supplementation and the Prevention of Clinical Cardiovascular Disease,” *Circulation*, vol. 135, no. 15, Apr. 2017.

[10] L. E. Lozada, A. Desai, K. Kevala, J.-W. Lee, and H.-Y. Kim, “Perinatal Brain Docosahexaenoic Acid Concentration Has a Lasting Impact on Cognition in Mice,” *J. Nutr.*, p. jn254607, Aug. 2017.

[11] S. Layé, A. Nadjar, C. Joffre, and R. P. Bazinet, “Anti-Inflammatory Effects of Omega-3 Fatty Acids in the Brain: Physiological Mechanisms and Relevance to Pharmacology,” *Pharmacol. Rev.*, vol. 70, no. 1, pp. 12–38, Jan. 2018.

[12] E. Messamore and R. K. McNamara, “Detection and treatment of omega-3 fatty acid deficiency in psychiatric practice: Rationale and implementation,” *Lipids Health Dis.*, vol. 15, no. 1, pp. 1–13, 2016.

[13] M. Huan *et al.*, “Suicide attempt and n-3 fatty acid levels in red blood cells: A case control study in china,” *Biol. Psychiatry*, vol. 56, no. 7, pp. 490–496, Oct. 2004.

[14] M. R. Garland *et al.*, “Lipids and essential fatty acids in patients presenting with self-harm,” *Br. J. Psychiatry*, vol. 190, no. 2, pp. 112–117, Feb. 2007.

[15] R. K. McNamara *et al.*, “Abnormalities in the fatty acid composition of the postmortem orbitofrontal cortex of schizophrenic patients: Gender differences and partial normalization with antipsychotic medications,” *Schizophr. Res.*, vol. 91, no. 1–3, pp. 37–50, Mar. 2007.

[16] R. K. McNamara *et al.*, “Deficits in docosahexaenoic acid and associated elevations in the metabolism of arachidonic acid and saturated fatty acids in the postmortem orbitofrontal cortex of patients with bipolar disorder,” *Psychiatry Res.*, vol. 160, no. 3, pp. 285–299, Sep. 2008.

[17] R. K. McNamara *et al.*, “Selective Deficits in the Omega-3 Fatty Acid Docosahexaenoic Acid in the Postmortem Orbitofrontal Cortex of Patients with Major Depressive Disorder,” *Biol. Psychiatry*, vol. 62, no. 1, pp. 17–24, Jul. 2007.

[18] F. Ducrocq *et al.*, “Causal Link between n-3 Polyunsaturated Fatty Acid Deficiency and Motivation Deficits,” *Cell Metab.*, Mar. 2020.

[19] M. L. Jacobs, H. A. Faizi, J. A. Peruzzi, P. M. Vlahovska, and N. P. Kamat, “EPA and DHA differentially modulate membrane elasticity in the presence of cholesterol,” *Biophys. J.*, vol. 120, no. 11, pp. 2317–2329, Jun. 2021.

[20] B. Antonny, S. Vanni, H. Shindou, and T. Ferreira, “From zero to six double bonds: Phospholipid unsaturation and organelle function,” *Trends in Cell Biology*, vol. 25, no. 7. Elsevier Ltd, pp. 427–436, Jul-2015.

[21] A. De Santis, Y. Varela, J. Sot, G. D'Errico, F. M. Goñi, and A. Alonso, "Omega-3 polyunsaturated fatty acids do not fluidify bilayers in the liquid-crystalline state," *Sci. Rep.*, vol. 8, no. 1, p. 16240, Dec. 2018.

[22] K. R. Levental *et al.*, "Polyunsaturated Lipids Regulate Membrane Domain Stability by Tuning Membrane Order," *Biophys. J.*, vol. 110, no. 8, pp. 1800–1810, Apr. 2016.

[23] S. R. Shaikh and M. Edidin, "Polyunsaturated fatty acids and membrane organization: elucidating mechanisms to balance immunotherapy and susceptibility to infection," *Chem. Phys. Lipids*, vol. 153, no. 1, pp. 24–33, May 2008.

[24] S. R. Wassall and W. Stillwell, "Polyunsaturated fatty acid–cholesterol interactions: Domain formation in membranes," *Biochim. Biophys. Acta - Biomembr.*, vol. 1788, no. 1, pp. 24–32, Jan. 2009.

[25] K. Tada, E. Miyazaki, M. Goto, N. Tamai, H. Matsuki, and S. Kaneshina, "Barotropic and thermotropic bilayer phase behavior of positional isomers of unsaturated mixed-chain phosphatidylcholines," *Biochim. Biophys. Acta - Biomembr.*, vol. 1788, no. 5, pp. 1056–1063, May 2009.

[26] Y. F. Dufrêne, D. Martínez-Martín, I. Medalsy, D. Alsteens, and D. J. Müller, "Multiparametric imaging of biological systems by force-distance curve–based AFM," *Nat. Methods*, vol. 10, no. 9, pp. 847–854, Sep. 2013.

[27] D. Alsteens, D. J. Müller, and Y. F. Dufrêne, "Multiparametric Atomic Force Microscopy Imaging of Biomolecular and Cellular Systems," *Acc. Chem. Res.*, vol. 50, no. 4, pp. 924–931, Apr. 2017.

[28] M. Lekka, P. Laidler, D. Gil, J. Lekki, Z. Stachura, and A. Z. Hrynkiewicz, "Elasticity of normal and cancerous human bladder cells studied by scanning force microscopy," *Eur. Biophys. J.*, vol. 28, no. 4, pp. 312–316, May 1999.

[29] J. L. Hutter and J. Bechhoefer, "Calibration of atomic-force microscope tips," *Rev. Sci. Instrum.*, vol. 64, no. 7, pp. 1868–1873, Jul. 1993.

[30] J. Domke, S. Dannöhl, W. J. Parak, O. Müller, W. K. Aicher, and M. Radmacher, "Substrate dependent differences in morphology and elasticity of living osteoblasts investigated by atomic force microscopy," *Colloids Surfaces B Biointerfaces*, vol. 19, no. 4, pp. 367–379, Dec. 2000.

[31] H.-J. Butt, B. Cappella, and M. Kappl, "Force measurements with the atomic force microscope: Technique, interpretation and applications," *Surf. Sci. Rep.*, vol. 59, no. 1–6, pp. 1–152, Oct. 2005.

[32] M. J. Rosenbluth, W. A. Lam, and D. A. Fletcher, “Force Microscopy of Nonadherent Cells: A Comparison of Leukemia Cell Deformability,” *Biophys. J.*, vol. 90, no. 8, pp. 2994–3003, Apr. 2006.

[33] K. D. Costa, “Single-Cell Elastography: Probing for Disease with the Atomic Force Microscope,” *Dis. Markers*, vol. 19, no. 2–3, pp. 139–154, 2004.

[34] V. Paketuryte *et al.*, “Uncertainty in protein–ligand binding constants: asymmetric confidence intervals versus standard errors,” *Eur. Biophys. J.*, vol. 50, no. 3–4, pp. 661–670, 2021.

[35] T. Parasassi, E. K. Krasnowska, L. Bagatolli, and E. Gratton, “Laurdan and Prodan as Polarity-Sensitive Fluorescent Membrane Probes,” *J. Fluoresc.*, vol. 8, no. 4, pp. 365–373, 1998.

[36] D. Van Der Spoel, E. Lindahl, B. Hess, G. Groenhof, A. E. Mark, and H. J. C. Berendsen, “GROMACS: Fast, flexible, and free,” *J. Comput. Chem.*, vol. 26, no. 16, pp. 1701–1718, Dec. 2005.

[37] E. Apol *et al.*, “GROMACS USER MANUAL,” 1991.

[38] S. J. Marrink, H. J. Risselada, S. Yefimov, D. P. Tieleman, and A. H. de Vries, “The MARTINI Force Field: Coarse Grained Model for Biomolecular Simulations,” *J. Phys. Chem. B*, vol. 111, no. 27, pp. 7812–7824, Jul. 2007.

[39] T. A. Wassenaar, H. I. Ingólfsson, R. A. Böckmann, D. P. Tieleman, and S. J. Marrink, “Computational Lipidomics with *insane* : A Versatile Tool for Generating Custom Membranes for Molecular Simulations,” *J. Chem. Theory Comput.*, vol. 11, no. 5, pp. 2144–2155, May 2015.

[40] G. Bussi, D. Donadio, and M. Parrinello, “Canonical sampling through velocity rescaling,” *J. Chem. Phys.*, vol. 126, no. 1, p. 014101, Jan. 2007.

[41] M. Parrinello and A. Rahman, “Polymorphic transitions in single crystals: A new molecular dynamics method,” *J. Appl. Phys.*, vol. 52, no. 12, pp. 7182–7190, Dec. 1981.

[42] M.-L. Jobin *et al.*, “Impact of membrane lipid polyunsaturation on dopamine D2 receptor ligand binding 1 and signaling 2,” *BioRxiv*.

[43] K. Czamara, K. Majzner, M. Z. Pacia, K. Kochan, A. Kaczor, and M. Baranska, “Raman spectroscopy of lipids: a review,” *J. Raman Spectrosc.*, vol. 46, no. 1, pp. 4–20, Jan. 2015.

[44] H. Wu, J. V. Volponi, A. E. Oliver, A. N. Parikh, B. A. Simmons, and S. Singh, “In vivo lipidomics using single-cell Raman spectroscopy,” *Proc. Natl. Acad. Sci. U. S. A.*, vol. 108, no. 9, pp. 3809–3814, Mar. 2011.

[45] H. Rosales-Solano, V. Galievsky, K. Murtada, P. V. Radovanovic, and J. Pawliszyn, “Profiling of Unsaturated Lipids by Raman Spectroscopy Directly on Solid-Phase Microextraction Probes,” *Anal. Chem.*, vol. 94, no. 2, pp. 606–611, Jan. 2022.

[46] D. J. Müller and Y. F. Dufrêne, “Atomic force microscopy as a multifunctional molecular toolbox in nanobiotechnology,” pp. 261–269.

[47] Y. F. Dufrêne *et al.*, “Imaging modes of atomic force microscopy for application in molecular and cell biology,” *Nat. Nanotechnol.*, vol. 12, no. 4, pp. 295–307, Apr. 2017.

[48] M. Krieg *et al.*, “Atomic force microscopy-based mechanobiology,” *Nat. Rev. Phys.*, vol. 1, no. 1, pp. 41–57, Jan. 2019.

[49] G. J. Blanchard and J. V. Busik, “Interplay between Endothelial Cell Cytoskeletal Rigidity and Plasma Membrane Fluidity,” *Biophys. J.*, vol. 112, no. 5, pp. 831–833, Mar. 2017.

[50] E. G. Kelley, P. D. Butler, R. Ashkar, R. Bradbury, and M. Nagao, “Scaling relationships for the elastic moduli and viscosity of mixed lipid membranes,” *Proc. Natl. Acad. Sci.*, vol. 117, no. 38, pp. 23365–23373, Sep. 2020.

[51] R. N. McElhaney, “The use of differential scanning calorimetry and differential thermal analysis in studies of model and biological membranes,” *Chem. Phys. Lipids*, vol. 30, no. 2–3, pp. 229–259, May 1982.

[52] A. Shibata, Y. Kiba, N. Akati, K. Fukuzawa, and H. Terada, “Molecular characteristics of astaxanthin and β-carotene in the phospholipid monolayer and their distributions in the phospholipid bilayer,” *Chem. Phys. Lipids*, vol. 113, no. 1–2, pp. 11–22, Nov. 2001.

[53] J. P. Douliez, A. Léonard, and E. J. Dufourc, “Restatement of order parameters in biomembranes: calculation of C-C bond order parameters from C-D quadrupolar splittings,” *Biophys. J.*, vol. 68, no. 5, pp. 1727–1739, May 1995.

[54] T. J. Piggot, Á. Piñeiro, and S. Khalid, “Correction to Molecular Dynamics Simulations of Phosphatidylcholine Membranes: A Comparative Force Field Study,” *J. Chem. Theory Comput.*, vol. 13, no. 4, pp. 1862–1865, Apr. 2017.

[55] L. S. Vermeer, B. L. de Groot, V. Réat, A. Milon, and J. Czaplicki, “Acyl chain order parameter profiles in phospholipid bilayers: computation from molecular dynamics simulations and comparison with 2H NMR experiments,” *Eur. Biophys. J.*, vol. 36, no. 8, pp. 919–931, Nov. 2007.

[56] Y. Wang, P. Gkeka, J. E. Fuchs, K. R. Liedl, and Z. Cournia, “DPPC-cholesterol phase diagram using coarse-grained Molecular Dynamics simulations,” *Biochim. Biophys. Acta* -

Biomembr., vol. 1858, no. 11, pp. 2846–2857, Nov. 2016.

[57] N. Michaud-Agrawal, E. J. Denning, T. B. Woolf, and O. Beckstein, "MDAnalysis: A toolkit for the analysis of molecular dynamics simulations," *J. Comput. Chem.*, vol. 32, no. 10, pp. 2319–2327, Jul. 2011.

[58] M. Pinot *et al.*, "Polyunsaturated phospholipids facilitate membrane deformation and fission by endocytic proteins," *Science (80-.).*, vol. 345, no. 6197, pp. 693–697, Aug. 2014.

[59] H. Barelli and B. Antonny, "Lipid unsaturation and organelle dynamics," *Current Opinion in Cell Biology*, vol. 41. Elsevier Ltd, pp. 25–32, Aug-2016.

[60] J. E. Mellor, J. D. E. Laugharne, and M. Peet, "Schizophrenic symptoms and dietary intake of n−3 fatty acids," *Schizophr. Res.*, vol. 18, no. 1, pp. 85–86, Dec. 1995.

[61] G. P. Amminger *et al.*, "Long-Chain ω-3 Fatty Acids for Indicated Prevention of Psychotic Disorders," *Arch. Gen. Psychiatry*, vol. 67, no. 2, p. 146, Feb. 2010.

[62] F. Darios and B. Davletov, "Omega-3 and omega-6 fatty acids stimulate cell membrane expansion by acting on syntaxin 3," *Nature*, vol. 440, no. 7085, pp. 813–817, Apr. 2006.

[63] A. Tixier-Vidal, R. Picart, C. Loudes, and A. F. Bauman, "Effects of polyunsaturated fatty acids and hormones on synaptogenesis in serum-free medium cultures of mouse fetal hypothalamic cells," *Neuroscience*, vol. 17, no. 1, pp. 115–132, Jan. 1986.

[64] E. Marza *et al.*, "Polyunsaturated Fatty Acids Influence Synaptojanin Localization to Regulate Synaptic Vesicle Recycling," *Mol. Biol. Cell*, vol. 19, no. 3, pp. 833–842, Mar. 2008.

[65] W. Stillwell and S. R. Wassall, "Docosahexaenoic acid : membrane properties of a unique fatty acid," *Chem. Phys. Lipids*, vol. 126, pp. 1–27, 2003.

[66] M. Carrillo-Tripp and S. E. Feller, "Evidence for a mechanism by which ω-3 polyunsaturated lipids may affect membrane protein function," *Biochemistry*, vol. 44, no. 30, pp. 10164–10169, 2005.

[67] C. Tessier *et al.*, "Membrane lipidomics in schizophrenia patients : a correlational study with clinical and cognitive manifestations," vol. 6, no. 10, pp. e906-8, 2016.

[68] W. Rawicz, K. C. Olbrich, T. McIntosh, D. Needham, and E. A. Evans, "Effect of chain length and unsaturation on elasticity of lipid bilayers," *Biophys. J.*, vol. 79, no. 1, pp. 328–339, 2000.

[69] V. Vitkova, D. Mitkova, and G. Staneva, "Lyso- and omega-3-containing phosphatidylcholines alter the bending elasticity of lipid membranes," *Colloids Surfaces A Physicochem. Eng. Asp.*, vol. 460, pp. 191–195, Oct. 2014.

[70] M. L. Tiberti, B. Antonny, and R. Gautier, “The transbilayer distribution of polyunsaturated phospholipids determines their facilitating effect on membrane deformation,” *Soft Matter*, vol. 16, no. 7, pp. 1722–1730, Feb. 2020.

[71] M. T. Hyvönen and P. T. Kovanen, “Molecular dynamics simulations of unsaturated lipid bilayers: effects of varying the numbers of double bonds,” *Eur. Biophys. J.*, vol. 34, no. 4, pp. 294–305, Jun. 2005.

[72] R. W. Evans, M. A. Williams, and J. Tinoco, “Surface areas of 1-palmitoyl phosphatidylcholines and their interactions with cholesterol,” *Biochem. J.*, vol. 245, no. 2, pp. 455–462, Jul. 1987.

[73] K. R. Levental *et al.*, “Lipidomic and biophysical homeostasis of mammalian membranes counteracts dietary lipid perturbations to maintain cellular fitness,” *Nat. Commun.*, vol. 11, no. 1, Dec. 2020.

[74] H. Ichimori, T. Hata, H. Matsuki, and S. Kaneshina, “Effect of unsaturated acyl chains on the thermotropic and barotropic phase transitions of phospholipid bilayer membranes,” *Chem. Phys. Lipids*, vol. 100, no. 1–2, pp. 151–164, Jul. 1999.

[75] G. Wang, S. Li, H. Lin, E. E. Brumbaugh, and C. Huang, “Effects of Various Numbers and Positions of cisDouble Bonds in the sn-2 Acyl Chain of Phosphatidylethanolamine on the Chain-melting Temperature,” *J. Biol. Chem.*, vol. 274, no. 18, pp. 12289–12299, Apr. 1999.

[76] F. Lolicato *et al.*, “Membrane-Dependent Binding and Entry Mechanism of Dopamine into Its Receptor,” *ACS Chem. Neurosci.*, vol. 11, no. 13, pp. 1914–1924, 2020.